Characteristics of terahertz coherent transition radiation generated from picosecond ultrashort electron bunches*

Liu Wen-Xin(刘文鑫)†, Tang Chuan-Xiang(唐传祥), and Huang Wen-Hui(黄文会)

Department of Engineering Physics, Tsinghua University, Beijing 100084, *China*
Key Laboratory of Particle & Radiation Imaging (Tsinghua University), Ministry of Education, Tsinghua University, Beijing 100084, *China*
Key Laboratory of High Energy Radiation Imaging Fundamental Science for National Defense, Tsinghua University, Beijing 100084, *China*

(Received 15 July 2009; revised manuscript received 21 December 2009)

This paper presents a method of generating terahertz (THz) coherent transition radiation (CTR) from picosecond ultrashort electron bunches including single and train bunches, which are produced by a photocathode radio frequency gun. The radiation characteristics of THz CTR including formation factor and energy spectrum are analysed in detail. With the help of a 2-dimensional particle-in-cell simulation, the radiation characteristics including power, energy and magnetic field are analysed. The results show that the radiation frequency can be adjusted by tuning the repetition frequency of the train bunch and the energy can be enhanced with the train bunches.

Keywords: coherent transition radiation, photocathode radio-frequency gun, ultrashort electron bunches, particle-in-cell

PACC: 2925E, 4260H

1. Introduction

Terahertz (THz) sources, a currently active research area, are of importance in a variety of applications such as far-infrared spectroscopy, medical and industrial imaging, biomedical research and material science.[1−3] Various schemes for generating THz waves have been employed, such as quantum cascade lasers,[4] ultrafast laser pulses[5] and vacuum electron devices,[6] etc. Among the various generations of THz wave, transition radiation (TR) as a THz source has a unique performance for its broadband. TR[7,8] is produced by relativistic charged particles when they cross the interface of two media of different dielectric constants. To analyse the characteristics of TR, some theories[9−11] have been developed, such as wake field theory, vector electromagnetic theory and image methods, etc. Moreover, some methods have been used to generate THz TR. Nikoghosyanac *et al.*[12] observed TR generated by short optical pulses crossing the boundary between linear and non-linear materials. Leemans *et al.*[13] and Plateau *et al.*[14] made use of an ultrashort laser driving a high intensity of plasma for the generation of THz coherent transition radiation (CTR). Hemsing *et al.*[15] presented a novel method of generating CTR with a helical microbunched beam. Recently, it was reported that an ultrabroadband THz source based on CTR is produced by ultrashort electron bunches.[16] However, to improve the performances of CTR, it is necessary to find some efficient methods to enhance it.

As we all know, coherent radiation occurs at wavelengths longer than, or comparable to, the bunch length of an electron beam, with an intensity that scales with N^2, where N is the number of electrons in the bunch, and typically ranges from 10^8–10^9 for an electron accelerator. The radiation pulse created by such a bunch can be subpicosecond in time and therefore contains coherent spectral content up to a few THz; the radiation of a single cycle can reach $\sim$100 μJ.[17] In this paper, THz CTR generated from train picosecond relativistic ultrashort electron bunches is presented, and the characteristics are analysed with numerical calculations and particle-in-cell (PIC) simulations.

This paper is organized as follows: the basic descriptions of TR including a single electron, single and

*Project supported by the Key Program of National Natural Science Foundation of China (Grant No. 10705050), National Natural Science Foundation of China (Grant Nos. 10875070, 10805031, and 10905032), by China Postdoctoral Science Foundation (Grant No. 20080440031) and China Postdoctoral Special Science Foundation (Grant No. 200902088).

†Corresponding author. E-mail: lwenxin@mail.tsinghua.edu.cn

© 2010 Chinese Physical Society and IOP Publishing Ltd

train of electron bunches are given in Section 2. The radiation characteristics by numerical calculations are analysed and compared in Section 3. The results of PIC simulations for single and train bunches are described in Section 4. The experimental setup for THz detection is described in Section 5, and some conclusions are given in Section 6.

2. Theory

2.1. Basic description of transition radiation

TR, first considered by Frank and Ginzburg,[11] is produced by the passage of charged particles through the interface between media with different dielectric constants and has been studied both theoretically and experimentally. In the present work, we consider that the TR is produced by a single bunch and train bunches, respectively.

Let us consider a current source moving toward an interface of vacuum and dielectric material with permittivity ε with velocity v and an angle of incidence ψ, as shown in Fig. 1, where k is a wave number locating in the observation plane consisting of horizontal $\boldsymbol{q}$ and normal directions $\boldsymbol{n}$, ϕ is an angle between the incidence plane and observation plane. For the general analysis of TR characteristics produced by cases of electron sources, a normalized formation of current density is introduced and represented as follows:

$$|\bar{J}(r,\omega)| = |\int_{-\infty}^{\infty} j(r,t)\mathrm{e}^{\mathrm{i}\,\omega t}\mathrm{d}t|/|ev|, \tag{1}$$

where $j(r,t)$ is the current distribution as a function of time t, e is the charge, ω is the angular frequency, v is the velocity of the electron bunch.

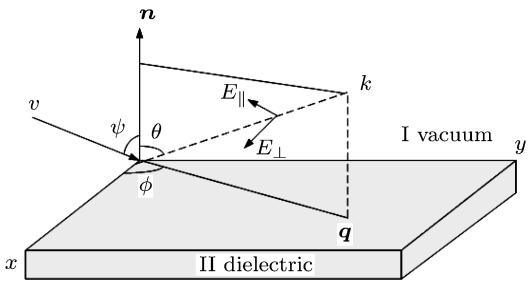


Fig. 1. Illustration of electric field and wave number geometry.

The electric field in the observation plane is divided into vertical and horizontal directions, so the radiation energy with the current source can be obtained through redundant deductions and is represented as follows:

$$\frac{\mathrm{d}^2W_{\parallel}}{\mathrm{d}\Omega\mathrm{d}\omega}(\omega,\psi,\theta,\varphi) = \frac{\mathrm{d}^2W'_{\parallel}}{\mathrm{d}\Omega\mathrm{d}\omega}\cdot|\bar{J}(r,\omega)|^2, \tag{2}$$

$$\frac{\mathrm{d}^2W_{\perp}}{\mathrm{d}\Omega\mathrm{d}\omega}(\omega,\psi,\theta,\varphi) = \frac{\mathrm{d}^2W'_{\perp}}{\mathrm{d}\Omega\mathrm{d}\omega}\cdot|\bar{J}(r,\omega)|^2, \tag{3}$$

where

$$\frac{\mathrm{d}^2W'_{\parallel}}{\mathrm{d}\Omega\mathrm{d}\omega}(\omega,\psi,\theta,\varphi) = \frac{e^2}{\pi^2 c}\cdot\frac{1}{\sin^2\theta}\cdot\frac{\beta^2\cos^2\theta\cos^2\psi|\varepsilon-1|^2}{A^2}\cdot\left[\frac{\sin^2\theta(1-\beta D+\beta C-\beta^2\cos^2\psi)-\beta^2 DC}{B}\right]^2,$$

$$\frac{\mathrm{d}^2W'_{\perp}}{\mathrm{d}\Omega\mathrm{d}\omega}(\omega,\psi,\theta,\varphi) = \frac{e^2}{\pi^2 c}\cdot\frac{\beta^6\sin^2\psi\cos^2\theta\sin^4\psi\sin^2\varphi|\varepsilon-1|^2}{A^2}\cdot\frac{1}{B^2},$$

in which c is the speed of light in vacuum, $\mathrm{d}^2W_{\parallel}/\mathrm{d}\Omega\mathrm{d}\omega$ and $\mathrm{d}^2W_{\perp}/\mathrm{d}\Omega\mathrm{d}\omega$ are the energy distributions of horizontal and vertical directions, respectively, and

$$A = (1-\beta\sin\theta\sin\psi\cos\varphi)^2 - \beta^2\cos^2\psi\cos^2\theta,$$

$$B = (1-\beta\sin\theta\sin\psi\cos\varphi+\beta\sqrt{\varepsilon-\sin^2\theta}\cos\psi)(\sqrt{\varepsilon-\sin^2\theta}+\varepsilon\cos\theta),$$

$$C = \sqrt{\varepsilon-\sin^2\theta}\cos\psi, \quad D = \sin\theta\sin\psi\cos\varphi.$$

From the expressions of Eqs. (2) and (3), we can get the total energy distribution formula as

$$\frac{\mathrm{d}^2W}{\mathrm{d}\Omega\mathrm{d}\omega} = \left(\frac{\mathrm{d}^2W'_{\perp}}{\mathrm{d}\Omega\mathrm{d}\omega}+\frac{\mathrm{d}^2W'_{\parallel}}{\mathrm{d}\Omega\mathrm{d}\omega}\right)|\bar{J}(r,\omega)|. \tag{4}$$

Obviously, the energy distribution varies with the normalized current source $|\bar{J}(r,\omega)|$, which will be discussed in the following subsection.

2.2. A single electron bunch

As all we know, coherent radiation occurs at wavelengths longer than, or comparable to, the bunch length $l_{\rm b}$ of the electron beam, with an intensity that scales with N^2, otherwise, that of incoherent radiation with scales N is emitted, where N is the number of electrons in the bunch. The current source of a single bunch $j(r,t)$ is given as follows:

$$j(r,t) = ev\sum_{i=1}^{N_{\rm b}} f(r-r_0), \tag{5}$$

where $f(r)$ is a shaped function and satisfies $\int_{-\infty}^{\infty} f(r-r_0){\rm d}r = 1$, r_0 is the centre of the electron bunch, and the number of electrons in a bunch $N_{\rm b}$ equals N. The Fourier transform (FT) of the current source is described as

$$\begin{aligned} |J(r,\omega)| &= ev\int_{-\infty}^{\infty}\sum_{i=1}^{N} f(r-r_0){\rm e}^{{\rm i}\,\omega t}{\rm d}t \\ &= evNM_{\rm b}{\rm e}^{{\rm i}\,\omega t_0}, \end{aligned} \tag{6}$$

where $M_{\rm b}(\omega)$ is the form factor and represented as

$$M_{\rm b}(\omega) = \int_{-\infty}^{\infty} f(r){\rm e}^{{\rm i}\,\omega t}{\rm d}t. \tag{7}$$

From Eqs. (6) and (7), we get the normalized current source

$$|\bar{J}(r,\omega)| = |J(r,\omega)|/|ev| = NM_{\rm b}. \tag{8}$$

Substituting Eq. (8) into Eqs. (2) and (3), we obtain the energy distribution of the single bunch as:

$$\left.\frac{{\rm d}^2W}{{\rm d}\Omega{\rm d}\omega}\right|_{\rm sb} = \left[\frac{{\rm d}^2W_{\parallel}}{{\rm d}\Omega{\rm d}\omega} + \frac{{\rm d}^2W_{\perp}}{{\rm d}\Omega{\rm d}\omega}\right](NM_{\rm b})^2. \tag{9}$$

Obviously, from Eq. (9), we know that the radiation energy is in proportion to $(NM_{\rm b})^2$ and sensitive to form factor.

As an example, we consider a bunch with Gaussian and rectangular distributions, respectively. Firstly, the bunch is a Gaussian distribution $f(z) = \exp(-z^2/2\sigma_z^2)/(\sqrt{2\pi}\sigma_z)$, and the form factor becomes[18]

$$M_{\rm b}(\omega,\sigma_z) = \exp\left(-\frac{1}{2}\frac{\omega^2}{c^2}\sigma_z^2\right), \tag{10}$$

in which σ_z is a standard width. Secondly, a rectangular function ${\rm Re}\,ct(z/l)$ describes a bunch distribution given as follows:

$${\rm Re}\,ct(z/l) = \begin{cases} 1, & -l/2 \le z \le l/2, \\ 0, & |z| > l/2, \end{cases} \tag{11}$$

where l is the length of the bunch, and its form factor is depicted as

$$M_{\rm b}(\omega,l) = \frac{\sin(\omega l/2c)}{\omega l/2c}. \tag{12}$$

From Eqs. (11) and (12), the maximum value of the form factor equals 1.0 when ω is close to 0; however, it is not an operation frequency. The form factor $M_{\rm b}$ equals 1 when the bunch is a delta function $f(z) = \delta(z)$; the radiation power or energy can be obtained as the maximum value.

2.3. Train of electron bunches

Assuming that the current source consists of a uniform and finite train (macropulse) of bunches cotaining $N_{\rm m}$ electrons injected periodically at frequency $\omega_{\rm b}$ into the interaction region, in which all bunches have the same pulse shape function $f(r-r_{0j})$ ($j = 1,\ldots,N_{\rm m}$) and the same number of electrons, $N_{{\rm b}j} = N_{\rm b}$, the current source can be expressed as[19]

$$j(r,t) = ev\sum_{j=0}^{N_{\rm m}-1}\sum_{n=1}^{N_{{\rm b}j}} f(r-r_{0j})\delta(r-vt), \tag{13}$$

where $t = t_0 + j\cdot 2\pi/\omega_{\rm b}$, and r_{0j} is the centre of the j-th bunch. Inserting the current source Eq. (13) into the FT, we obtain the frequency domain current source as

$$\begin{aligned} J(r,\omega) &= ev\sum_{j=0}^{N_{\rm m}-1}\sum_{n=1}^{N_{{\rm b}j}}\int f(r-r_{0j})\delta(r-vt){\rm e}^{{\rm i}\,\omega t}{\rm d}t \\ &= evNM_{\rm M}(\omega)M_{\rm b}(\omega){\rm e}^{{\rm i}\,\omega t_0}, \end{aligned} \tag{14}$$

where $N = N_{\rm m}N_{\rm b}$, and

$$\begin{aligned} M_{\rm M}(\omega) &= \exp\left[-{\rm i}\,\pi(N_{\rm m}-1)\omega/\omega_{\rm b}\right] \\ &\quad\times\frac{\sin(N_{\rm m}\pi\omega/\omega_{\rm b})}{N_{\rm m}\sin(\pi\omega/\omega_{\rm b})} \end{aligned} \tag{15}$$

is the macrobunching factor. The form factor amplitude per bunch is obtained as

$$M_{\rm b}(\omega) = \int_{-\pi/\omega_{\rm b}}^{\pi/\omega_{\rm b}} f(r){\rm e}^{{\rm i}\,\omega t}{\rm d}t. \tag{16}$$

From Eq. (14), the normalized current source of train bunches is obtained as follows:

$$|\bar{J}(r,\omega)| = |J(r,\omega)|/|ev| = NM_{\rm b}M_{\rm M}, \tag{17}$$

then the energy distribution of train bunches is depicted as:

$$\left.\frac{{\rm d}^2W}{{\rm d}\Omega{\rm d}\omega}\right|_{\rm tb} = \left[\frac{{\rm d}^2W_{\parallel}}{{\rm d}\Omega{\rm d}\omega} + \frac{{\rm d}^2W_{\perp}}{{\rm d}\Omega{\rm d}\omega}\right](NM_{\rm b}M_{\rm M})^2. \tag{18}$$

Comparing Eq. (18) with that of the single bunch Eq. (9), we find that the remarkable difference of factor $M_{\rm M}$ is interesting and of practical significance, for which there are multiple peaks of equal amplitude "1" and a bandwidth $N_{\rm b}^{-1}$ at all harmonic frequencies $n\omega_{\rm b}$, where $n = N_{\rm m}$ is the number of train bunches. Measurement of intensity of this periodical coherent system allows a further enhancement of $N_{\rm b}$ in comparison with that of incoherent radiation. On the other hand, it means that it is not essential that the electron beam is bunched at the radiation frequency ω. It can be bunched at any subharmonic of the radiation frequency $\omega = \omega_{\rm b}/n$, as long as there is a radiation process at frequency ω, and the microbunch has spectral components at this frequency. This means that narrow bandwidth intense THz radiation can be attained with a train of electron bunches.

3. Numerical analysis

In this section, the radiation characteristics for three cases of current sources are studied by numerical calculation, in which the energy and power distributions are analysed.

3.1. A single bunch

According to the experimental plan, the THz CTR experiment will be performed based on the photocathode radio frequency (RF) gun table at the Accelerator Laboratory of Tsinghua University. The ultrashort electron bunch is produced by a photocathode RF gun, which is similar to the traditional BNL/ATF 1.6-cell RF gun system, operating at a frequency of 2856 MHz. It is driven by a solid state femtosecond Ti:sapphire laser system composed of a Ti:sapphire passive mode-locked oscillator, a regenerative amplifier, a three-harmonic generator and an ultraviolet (UV) pulse stretcher. The UV pulse width can be changed from several hundred femtoseconds to 15 ps by the pulse stretcher, and the regenerative amplifier is capable of producing 2 mJ in the infrared region and, after the three-harmonic generator, $\sim$500 μJ in the UV region. The repetition rate of the laser system in the experiment is 10 Hz. By tuning the femtosecond laser system with the help of α-BBO crystal sequences, we can obtain the ps interval, nC ulstrashort of electron bunches.

In this subsection, we focus on the Gaussian and rectangular electron bunch; its form factors are illustrated in Fig. 2, respectively. From Fig. 2, we know that the Gaussian form factor is larger than the rectangular form factor when the radiation locates at the low frequency; this means that the maximum energy with the Gaussian beam can be obtained.

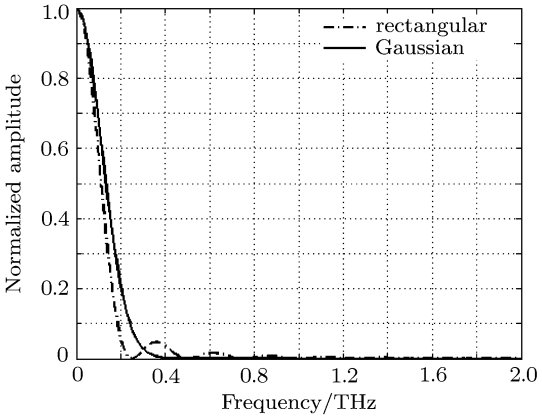


Fig. 2. Form factor.

Figure 3 is the energy distributions of a single bunch with different form factors at a fixed frequency of 1.0 THz and 0° incidence angle. Obviously, the maximum value of radiation energy can be obtained when the electron bunch distribution is a delta function with form factor 1. Otherwise, it will decreased when the electron bunch has another distribution.

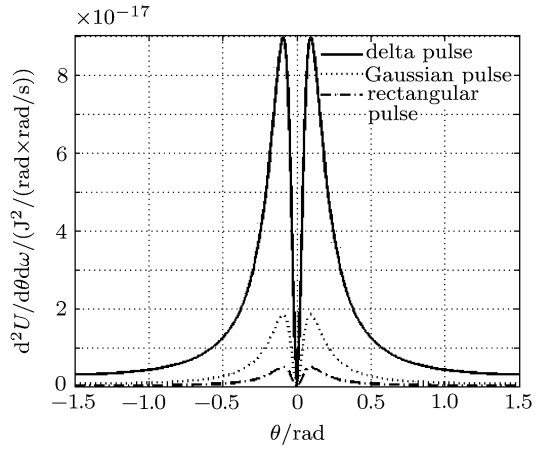


Fig. 3. Energy distribution of electron bunch with different formation factors with 0° incidence angle.

The 3D energy distribution as a function of frequency and observation angle θ is shown in Fig. 4, in which the electron bunch with 0° incidence angle is a Gaussian distribution. It shows that the radiation energy, which is symmetrical in the direction of observation angle, is focused on the lower frequency and decreases with increasing frequency.

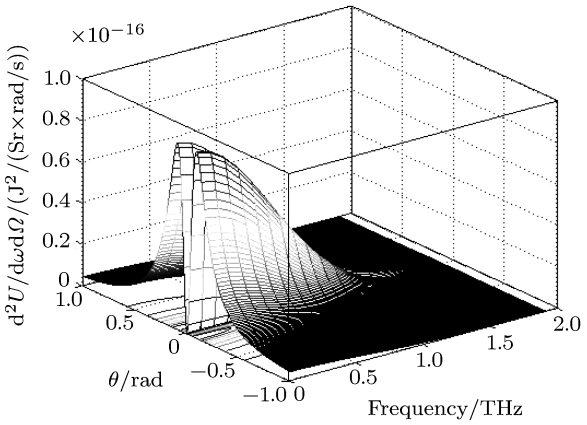


Fig. 4. Energy distribution of electron bunch versus frequency and observation angle at 0° incidence angle.

According to the energy distribution formalism with form factor Eq. (14), we integrate the solid angle of $\mathrm{d}\Omega = 2\pi \sin\theta \mathrm{d}\theta$, and obtain that of a Gaussian shape with different bunch lengths as plotted in Fig. 5. This shows that the intensity of the short bunch radiation energy is stronger than that of the long bunch. When the bunch charge is about 1.0 nC, we calculate that the total radiation energy, by integrating the frequency up to 2.0 THz, reaches about 113.6 μJ and the mean power with 10-Hz repetition rate is about 1.13 mW.

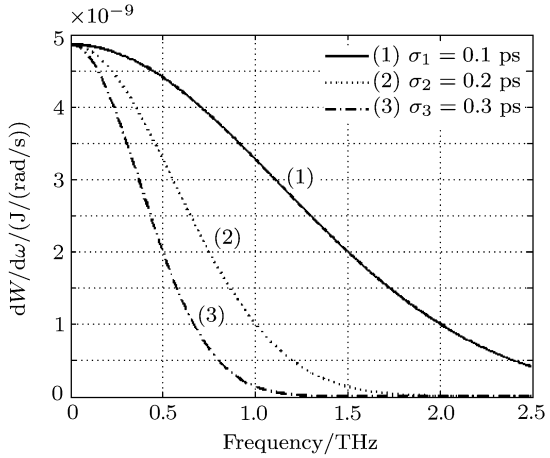


Fig. 5. Energy distribution versus frequency with different bunch lengths.

3.2. Train of bunches

A femtosecond laser driven system can produce an ultrashort pulse, the length of which is from 0.1 to several picoseconds. Pulse bunches can be produced by many methods,[20−24] such as modulation using the F-P interferometer pulse-shaping technique, four-wave mixing, a sequence of birefringent crystals and an electric optical modulation system, etc. In our experimental table, the pulse shapes are produced by α-BBO crystal sequences, which drive the photocathode RF gun for the generation of electron bunches.

According to the formula of $|M_{\mathrm{M}}(\omega)|$, the macropulse formation factor is plotted in Fig. 6. Obviously, the maximum value is 1 at a frequency of $f = nf_0$, where f_0 is the frequency of the bunch. Figure 7 is the form factor of train bunches in combinations of bunch shape and periodic bunch. It tells us that the frequency of the THz radiation wave can be chosen by adjusting the bunch frequency. According to Eq. (18), we consider that the distribution per bunch is a Gaussian one, and the radiation energy consisting of four bunches with repetition frequency 1.0 THz is about 487.4 μJ. Compared with the single bunch, we find that the radiation energy is remarkably enhanced at the bunch frequency.

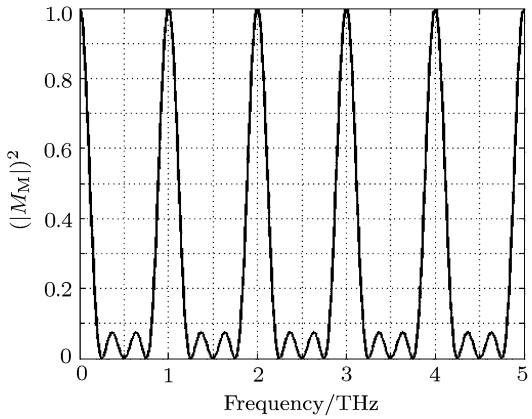


Fig. 6. The macropulse form factor.

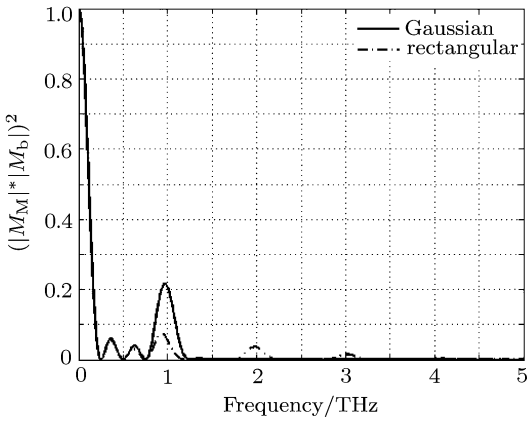


Fig. 7. Train of the form factor in cases of Gaussian and rectangular shape.

4. The PIC simulation

4.1. Descriptions of simulation geometry

The PIC simulations are performed with the CHIPIC code,[25] which is a finite-difference, time-domain code for simulating processes involving interactions between space charge and electromagnetic fields. With the help of the 2D PIC simulation, the characteristics of transition radiation including the radiation energy and field distribution as well as the interaction processes of electron bunches with the target can be observed. During the simulation, the commands 'foil' and 'film' are used when the target is a perfect conductor and dielectric material, respectively.

A simulation of the cylindrical geometry is shown in Fig. 8. The target is located at the right, and electron beam is emitted from the left perfect conductor. The interactions of the electron with the foil and the processes of radiation happen in the vacuum area, which is enclosed by a special region (called free space in PIC language), where the incident electro-magnetic waves can be absorbed. The operation area is divided into a mesh with rectangular cells ($\delta z = 0.025$ mm) in the radiation and another mesh size is just the thickness of the foil in the z-direction; the r-direction mesh size is uniform ($\delta r = 0.025$ mm).

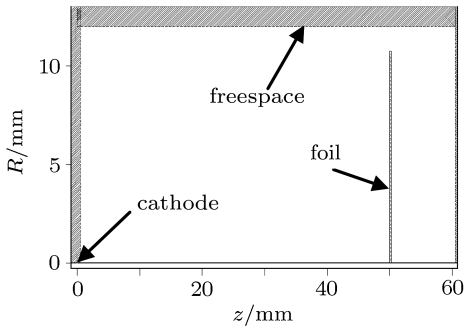


Fig. 8. Simulation geometry.

4.2. Descriptions of simulation parameters

The main parameters of the simulation are summarized in Table 1. The energy of the electron bunch is 5 MeV, and it can reach a higher energy when it is accelerated. The radius of the bunch is 0.5 mm, and it will be expanded due to the effect of space charge in the transmission. The charge and root-mean-square length of the single bunch are 1.0 nC and 0.2 ps, respectively. For the train bunches, the period is 1.0 ps and the number of bunches is four; the other parameters are the same as that of the single bunch. During the simulation, the current source will be varied when it is a single bunch and a train of bunches. As to the diagnostics, PIC allows us to observe a variety of physical quantities such as electromagnetic fields as functions of time and space, power outflow, and electron phasespace trajectories, etc. We can set the relevant detectors anywhere in the simulation area.

Table 1. Electron parameters.

	Gaussian	
	single	train
energy/MeV	5	5
radius/mm	0.5	0.5
charge/nC	1.0	4.0
σ_z/ps	0.2	0.2
period/ps	/	1.0

4.3. Simulation results

In this simulation, we firstly employ a single electron bunch passing through a thin titanium foil, considered a perfect conductor with a thickness of 0.25 mm. The electron bunch with charge 1.0 nC generated from the left cathode has a Gaussian profile and a length of $\sigma_z = 0.20$ ps. Comparing the wavelength of the 1.0 THz wave, we find that when the bunch length is less than that, the TR can be considered as coherent radiation.

The interaction processes of the ultrashort electron bunch shot at different run times with Ti foil can be observed through the distributions of all particles in phasespace, as shown in Figs. 9(a)–9(d). Figure 9(a) shows a single Gaussian bunch in the vacuum area moving toward the Ti foil. The bunch shape is not affected. Figure 9(b) displays the electron bunch located at the middle of the cathode and foil. It shows that the bunch shape is distorted. On the other hand, the shape of the single bunch shown in Fig. 9(c) is severely distorted compared to that in Fig. 9(b), since it is affected by the space charge, resulting in the distortion of bunch shape. Figure 9(d) just displays the electron bunch passing through the Ti foil; some electrons have entered into it, and some others are outside. Obviously, some electrons pass through the foil and some others are reflected. The distribution of the electron bunch is destroyed, and it becomes emanative.

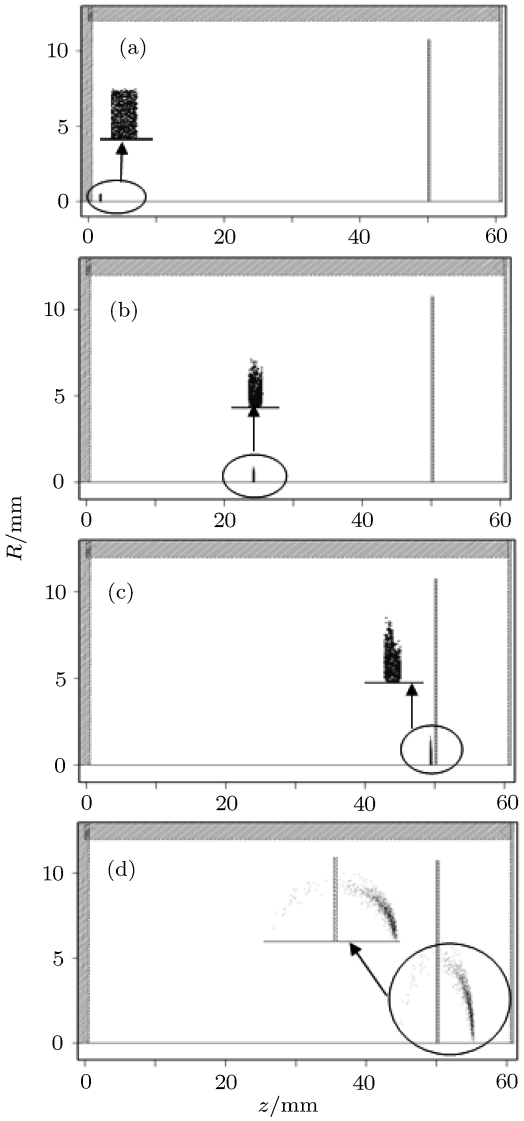


Fig. 9. Phase space for all particles of the single bunch. (a) 8.017 ps; (b) 83.120 ps; (c) 166.662 ps; (d) 189.446 ps.

Similarly, the interaction processes of train bunches in phase space are shown in Figs. 10(a)–10(d). At the left of the simulation geometry, there are four bunches generated from the cathode as shown in Fig. 10(a). The parameter and the shape per bunch are the same as that of the single bunch. When the train bunches reach the middle of the simulation geometry, the distributions of all particles in phase space are plotted in Fig. 10(b). Obviously, the shape per bunch is also influenced. The distributions of all particles close to the target are depicted in Fig. 10(c). Comparing the shapes of train bunches with that of the single bunch in Fig. 9(c), we find that the distortions of the former are more severe than those of the latter, since the shape changes of train bunches are affected not only by the space charge effect per bunch but also by the mutual influences among bunches. Figure 10(d) shows that a majority of electrons pass through the foil and some minority ones are reflected. This picture is similar to that of Fig. 9(d).

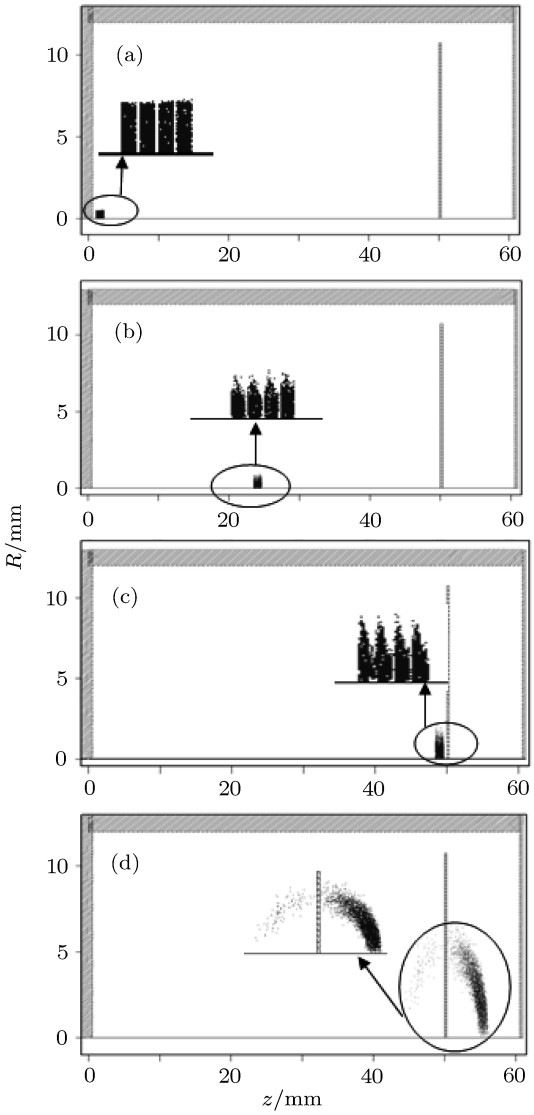


Fig. 10. Phase space for all particles of the train bunch. (a) 8.017 ps; (b) 83.120 ps; (c) 166.662 ps; (d) 189.446 ps.

Meanwhile, for observation of the radiation field, we place detectors at intervals of 1° in the observation plane with a radius of 48 mm relative to the foil centre. Normally, the observation point can be regarded as locating at the far field when d is much larger than $\gamma^2\lambda$, i.e., $d \gg \gamma^2\lambda$, where d is the distance between the observation point and the titanium foil, γ is the relativistic mass factor, and λ is the radiation wave length. Because of the limitation of computer performance, the simulation region is a finite area. In the present PIC simulation, the observation point d is 48 mm, which is about 160 times $\lambda = 0.3$ mm. Therefore, we

can consider that the observation point is located at far field. The FTs of the azimuth magnetic field B_φ for single and train bunches are shown in Figs. 11(a) and 11(b) respectively. Obviously, the peak of the magnetic field is a maximum at a frequency of bunch repetition rate of about 0.97 THz, and the amplitude of FT B_φ for train bunches is about 3.5 times that of single bunches.

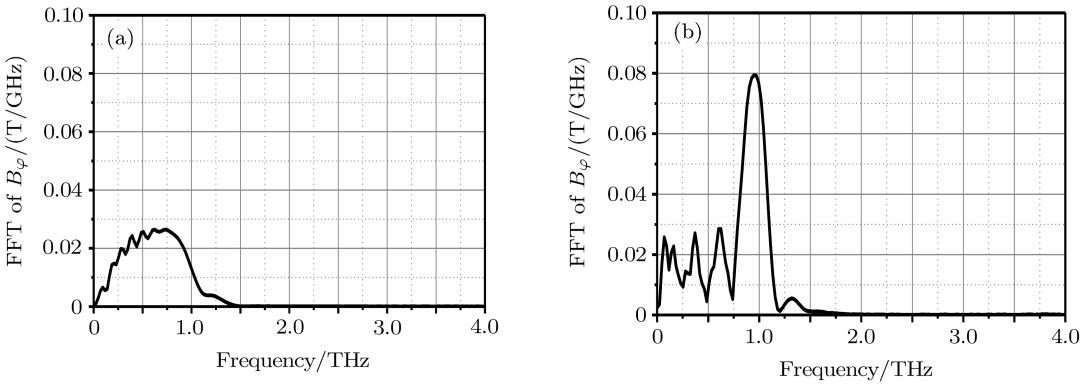


Fig. 11. Azimuth radiation magnetic field for a bunch: (a) single; (b) train.

For the observation of radiation power, we set a power line at $z = 2$ mm with the foil distance 48 mm, and obtain the power shown in Figs. 12(a) and 12(b). Obviously, the power of the train is larger than that of the single bunch. The radiation energy of train bunches is obtained by the integration of power about 477.3 μJ, and that of the single bunch is 109.7 μJ.

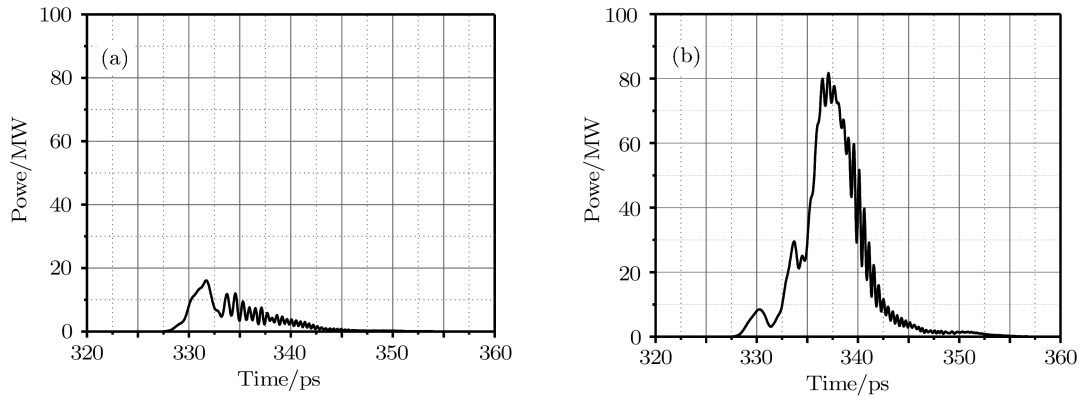


Fig. 12. Radiation power for a bunch: (a) single; (b) train.

The FTs of radiation power are displayed in Figs. 13(a) and 13(b), which correspond to those plotted in Figs. 12(a) and 12(b), respectively. During the PIC simulation, the frequency of radiation power is two times that of the radiation field, in which the central frequency is about 0.97 THz. The former one is shown in Fig. 13, in which the frequency of radiation power is close to 1.95 THz, moreover, the peak power of train bunches is larger than that of the single bunch: the former is 12.5 times that of the latter. The enhancement of peak power is close to $N_{\rm m}^2$ at the harmonics of repetition rate, this result is in good agreement with those reported in Ref. [26]. On the other hand, the space charge and transverse size are not considered, resulting in the simulation result being less than that of the theoretical calculation. The results indicate that the radiation power can be enhanced and the bandwidth can be adjusted by the help of tuning the repetition frequency of train bunches.

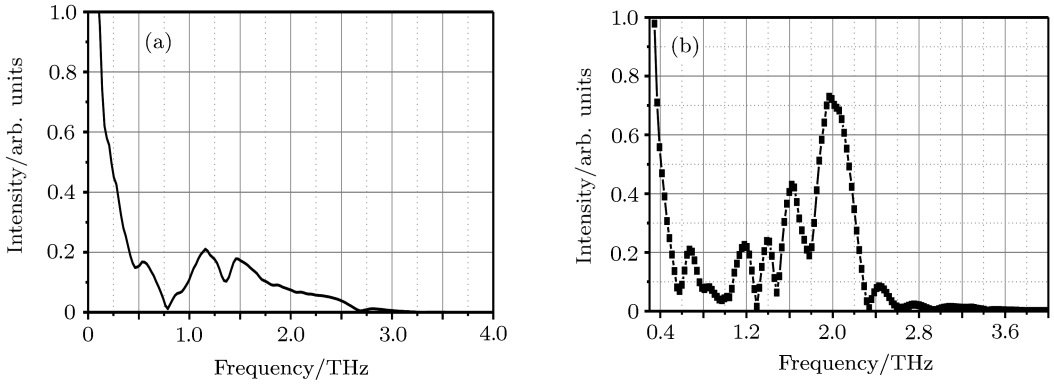


Fig. 13. The FTs of radiation power for a bunch: (a) single; (b) train.

5. The experimental setup for detecting THz

Single and periodic electron bunching are produced by the RF photocathode driven by the femosecond laser system, and the experimental setup for THz CTR is shown in Fig. 14. The bunching charge can be tested by an integration current transformer. When the THz wave escapes from the vacuum chamber, its frequency can be measured by the improved Martin–Purplett interferometer, shown in Fig. 14(a), and the intensity of THz CTR can be detected by Golay cell detector combinations with off-axis parabolic mirrors (OAP), shown in Fig. 14(b).

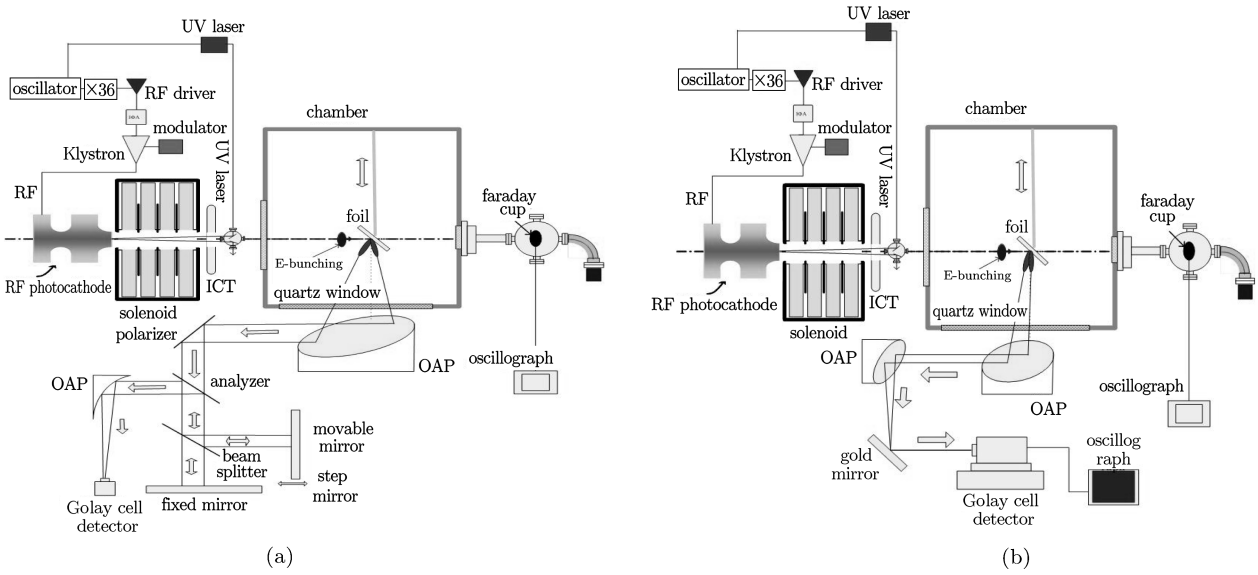


Fig. 14. The experimental setup: (a) frequency measurement; (b) power measurement.

6. Conclusions

This paper presents an approach to the enhancement of CTR intensity realized by periodic train bunches, and the THz CTR characteristics are analysed through numerical solutions and PIC simulations. For analysing the characteristics of TR generated from three cases of single and train bunches, the normalized current is introduced. The theoretical and PIC results show that the mW THz radiation can be generated from the CTR at the ps, nC bunches, the operation frequency can be adjusted and the radiation energy can be remarkably enhanced by the train bunches. The THz CTR experiment is underway.

References

[1] Siegel P H 2002 *IEEE Trans. Microwave Theory Tech.* **50** 910

[2] Yue W W, Wang W N, Zhao G Z, Zhang C L and Yan H T 2005 *Acta Phys. Sin.* **54** 3094 (in Chinese)

[3] Zhang X B and Shi W 2008 *Acta Phys. Sin.* **57** 4984 (in Chinese)

[4] Faist J, Capasso F, Sivco D L, Sirtori C, Hutchinson A L and Cho A Y 1994 *Science* **264** 553

[5] Hu Q L, Liu S B and Li W 2008 *Chin. Phys.* B **17** 1050

[6] Zhang K C, Wu Z H and Liu S G 2008 *Chin. Phys.* B **17** 3042

[7] Ginzburg V L and Frank I M 1946 *JETP* **16** 15

[8] Ter-Mikaelian M L 1972 *High-Energy Electromagnetic Processes in Condensed Media* (New York: Wiley-Interscience) p. 239

[9] Xiang D and Huang W 2005 *Nucl. Instrum. Methods Phys. Res. Section* A **553** 381

[10] Shkvarunets A G and Fiorito R B 2008 *Phys. Rev. ST Accel. Beams* **11** 012801

[11] Ginzburg V L and Tsytovich V N 1990 *Transition Radiation and Transition Scattering* (New York: Adam Hilger) p. 374

[12] Nikoghosyanac A S, Lazieva E M and Martirosyan R M 2004 *Int. Conf. on Infrared and Millimeter Waves and Terahertz Electronics* **1** 159

[13] Leemans W P, Tilborg J van and Faure J 2004 *Phys. Plasma* **11** 2899

[14] Plateau G R, Matlis N H and Albert O 2009 *AIP Conf. Proc.* **1086** 707

[15] Hemsing E and Rosenzweig J B 2009 *J. Appl. Phys.* **105** 093101

[16] Casalbuoni S, Schmidt B and Schmuser P 2009 *Phys. Rev. ST Accel. Beams* **12** 030705

[17] Shen Y, Watanabe T and Arena D A 2007 *Phys. Rev. Lett.* **99** 043901

[18] Chao A W and Tigner M 2006 *Accelerator Physics and Engineering* 3rd ed. (New York: World Scientific) p. 367

[19] Gover A and Dyunin E 2005 *Phys. Rev. ST Accel. Beams* **8** 030701

[20] Neumann J G and O'Shea P G 2003 *Nucl. Instrum. Methods Phys. Res. Section* A **507** 498

[21] Robinson T, O'Keeffe K and Landreman M 2007 *Opt. Lett.* **32** 2203

[22] Inoue T, Hiroishi J and Yagi T 2007 *Opt. Lett.* **32** 1596

[23] Bates H E, Alfano R R and Schille N 1979 *Appl. Opt.* **18** 947

[24] Radzewicz M J and Krasinski La Grone 1996 *Appl. Phys. Lett.* **69** 272

[25] Di J, Zhu D and Liu S 2005 *Electro-magnetic Field Algorithm of the CHIPIC Code*

[26] Korbly S E, Kesar A S and Sirigiri J R 2005 *Phys. Rev. Lett.* **94** 054803